frontiers | Frontiers in Energy Research

TYPE Original Research
PUBLISHED 01 October 2025
DOI 10.3389/fenrg.2025.1663842

OPEN ACCESS

EDITED BY
Mehmet Kadri Aydinol,
Middle East Technical University, Türkiye

REVIEWED BY
Mohamed Barakat Zakaria,
Tanta University, Egypt
Lujain Moazeen,
Damascus University, Syria

*CORRESPONDENCE
Rudolf Kiefer,
rudolf.kiefer@tdtu.edu.vn
Quoc Bao Le,
lequocbao@tdtu.edu.vn

RECEIVED 11 July 2025
ACCEPTED 16 September 2025
PUBLISHED 01 October 2025

CITATION
Delawary AR, Bubulinca C, Pechancová V, Kazantseva NE, Saha P, Kiefer R and Le QB (2025) Aerogel made of ternary metal sulfide $FeCo_2S_4$ and rGO enhanced with biowaste activated carbon and PANI for supercapacitor. *Front. Energy Res.* 13:1663842. doi: 10.3389/fenrg.2025.1663842

Aerogel made of ternary metal sulfide $FeCo_2S_4$ and rGO enhanced with biowaste activated carbon and PANI for supercapacitor

Ahmad Reshad Delawary[1], Constantin Bubulinca[1], Viera Pechancová[1], Natalia E. Kazantseva[1], Petr Saha[1], Rudolf Kiefer [2]* and Quoc Bao Le[1,3]*

[1]University Institute, Tomas Bata University in Zlín, Zlín, Czechia, [2]Conducting Polymers in Composites and Applications Research Group, Ton Duc Thang University, Ho Chi Minh City, Vietnam, [3]National Institute for Materials Advancement, Pittsburg State University, Pittsburg, KS, United States

Supercapacitors utilizing activated carbon derived from Brewer's spent grain (BSG) offer a sustainable and innovative solution for rapid energy storage and release. Pyrolysis using various activation techniques transforms biowastes into highly porous materials with large surface areas, making them ideal for supercapacitor applications. In this study, $FeCo_2S_4$ was synthesized and combined with reduced graphene oxide (rGO) to create an aerogel. Brewery biowaste activated carbon (AC) and polyaniline (PANI) were added to enhance the electrochemical properties of the composite electrode material. Those composites morphologies were observed via SEM. Their electrochemical properties were tested using CV, GCD and EIS. The electrochemical performance of the resulting rGO/AC/$FeCo_2S_4$@PANI composite was evaluated, achieving a high specific capacitance of 290.57 F/g at 0.5 A/g, comparable to that of the composite without AC. The small charge transfer resistance values of rGO/AC/$FeCo_2S_4$ required via full cell testing in this research showed the value of 1.498 Ω, suggesting superior retention. Therefore, AC significantly enhanced cycling stability, with the composite retaining 97.6% of its capacitance after 5,000 cycles.

KEYWORDS

supercapacitor, ternary metal sulfide, reduced graphene oxide, electrochemical composites, polyanilin

1 Introduction

Environmental concerns have driven global innovation, particularly in addressing waste from breweries, which account for over 10% of global beverage consumption. One emerging solution is the transformation of brewing bio-waste into electrodes for energy storage systems, a promising yet challenging approach (Le et al., 2024). Researchers have sought alternatives to fossil fuels in recent years, as these conventional energy sources contribute significantly to environmental degradation. Renewable energies such as solar and wind power have shown great promise; however, efficient

energy storage remains a critical challenge. Energy storage systems, including supercapacitors (SCs) and batteries, enable the capture and later use of power from these intermittent sources (Wei et al., 2011; Xu et al., 2013; Zhao and Zheng, 2015; Gao, 2017; Sapurina et al., 2021). Among these technologies, electrochemical supercapacitors are an up-and-coming power storage device class. Their advantages, such as high power density, excellent reversibility, long cycle life, and high intrinsic safety, make them well-suited for modern technological applications (Ma et al., 2009; Gong et al., 2013; Wang et al., 2019).

For the design of SC electrodes, carbon-based materials (Le et al., 2020), transition metal oxides (Abdullah et al., 2023), and conductive polymers (Rudolf et al., 2024) are most commonly employed. These materials enhance SC capacity through Faradaic reactions and charge separation at the electrode-electrolyte interfaces (Kiefer et al., 2023). Biowaste-derived activated carbon has emerged as a key material for supercapacitors. Recent advances focus on the use of porous carbon materials obtained from biomass sources such as rice husks (Teo et al., 2016), apple waste (Delewary et al., 2025), banana peels (Fasakin et al., 2018), walnut shells (Fu et al., 2020), plant leaves (Gopalakrishnan and Badhulika, 2020), wheat straw (Wang et al., 2020), cotton stalk (Abioye and Ani, 2015), and many other agricultural byproducts. Converting biowaste into high-performance porous carbon promotes sustainability by reducing pollution from conventional disposal methods, such as incineration, while improving resource efficiency. This recycling approach supports a circular economy by transforming waste into valuable electrode materials for energy storage. Biomass-derived carbon is chemically robust and cost-effective; however, its specific capacitance is generally limited. To improve the capacitance of SCs, heteroatoms such as oxygen, nitrogen, and sulfur can be introduced into the carbon matrix (Mohamed et al., 2014). Possess exceptional electrical properties but still face constraints, including restricted surface area and complex fabrication processes.

Researchers have recently developed nano-carbon materials and enhanced carbon composites (Basnayaka et al., 2017). While these materials exhibit excellent electrochemical performance in laboratory settings, their large-scale production remains challenging (Li et al., 2022). As a result, designing composites that integrate the strengths of individual components has become a major research focus (Bakhoum et al., 2022). Polyaniline (PANI) is one such material that has long been explored for SC applications. PANI offers several advantages as a conducting polymer, such as high reversibility, tunable electrical conductivity through synthesis conditions, safe processing, and excellent pseudocapacitance (Zhang et al., 2010). However, its poor cyclic stability, caused by mechanical degradation during the doping–dedoping process, limits its long-term performance in charge-discharge cycles (Le et al., 2024).

In this study, we report the synthesis of two-step activated carbon from brewer's spent grain (BSG) sourced from a local brewery in Zlín Province, Czechia. The preparation process is detailed in Supplementary Scheme S1. This approach represents an eco-friendly strategy, reducing environmental impact by converting biowaste into high-value materials. Using activated carbon (AC) derived from BSG offers a sustainable alternative to conventional SC electrode materials and can potentially lower production costs. Composites of rGO/$FeCo_2S_4$ and rGO/AC/$FeCo_2S_4$ were prepared via co-assembly, and their electrochemical properties were systematically evaluated to assess their potential as electrode materials for SC. It is well-known that rGO and AC can exhibit good EDLC but tend to have lower specific capacitance than the pseudocapacitive materials (Basnayaka et al., 2017). The $FeCo_2S_4$ would contribute to the composites' pseudocapacitance, they also a spacer to make the aerogel of the composite made of rGO and AC stable. PANI was conjugated into the composite via *in situ* polymerization to test the cell's compatibility and overall working performance. The resulting electrodes were evaluated in a 1M H_2SO_4 electrolyte. A symmetric supercapacitor assembled with the 1M H_2SO_4 electrolyte demonstrated excellent cycling stability, retaining 97.6% of its initial capacitance over 5,000 cycles.

2 Experimental

2.1 Materials

Synthetic graphite powder (<20 μm), potassium permanganate ($KMnO_4$ ≥ 99.0%), ammonium persulfate ($(NH_4)_2S_2O_8$, ≥ 98.0%), aniline, Manganese (II) chloride tetrahydrate ($MnCl_4.4H_2O$), perchloric acid ($HClO_4$, 70%), Cobalt (II) chloride hexahydrate ($CoCl_2.6H_2O$), Iron (II) chloride tetrahydrate ($FeCl_2.4H_2O$), urea ($CO(NH_2)_2$), potassium hydroxide (KOH), and sodium sulfide (Na_2S) were products of Sigma-Aldrich. Sulfuric acid (96%), hydrochloric acid, hydrogen peroxide solution (30%), and all solvents were purchased from local companies PENTA and VWR Chemicals. All chemicals were used without further purification except the aniline, which must be distilled twice before use.

2.2 Characterization techniques

The crystal structure of $FeCo_2S_4$ was analyzed via X-ray powder diffraction (XRD) patterns employing a Cu-Kα radiation source from a D8 Advance Brucker powder diffractometer. The chemical composition was identified by ATR-FTIR spectroscopy using Nicolet iS10 (Thermo Scientific), which was equipped with an ATR sampling accessory and a Ge crystal plate. The composites' carbon, hydrogen, and nitrogen contents were determined by elemental analysis (EA).

The material morphologies were characterized by a NANOSEM 450 (FEI, United States) scanning electron microscope (SEM) operated at 5 kV under 90 Pa pressure. The samples were ultrasonically dispersed in water (0.5 wt%) using the Ultrasonic processors 500 W, drop-cast onto 300 mesh copper grids, and gently dried inside the Memmert oven UF30.

2.3 Synthesis

2.3.1 $FeCo_2S_4$ synthesis

3 mmol of $CoCl_2.6H_2O$ (0.714 g) was mixed with 1.5 mmol of $FeCl_2.4H_2O$ (0.298 g) and 37.5 mmol of $CO(NH_2)_2$ (2.252 g) in 60 mL DI water. The mixture was stirred until completely dissolved and then transferred into an 80 mL autoclave for hydrothermal treatment at 120 °C for 12 h. Hence, the autoclave was cooled to

room temperature to collect the precipitate (Chen et al., 2024). The precipitate was rinsed with DI water and ethanol several times and dried overnight under a vacuum at 70 °C to receive 0.43 g gray powder of pre-annealed $FeCo_2O_4$. 0.4 g of that gray powder was mixed with Na_2S (7.1 mmol, 0.555 g) and 60 mL in the autoclave. The mixture was gently stirred and hydrothermally treated at 160 °C for 12 h. The intermediate was collected, rinsed with H_2O, EtOH, and dried inside the oven at 60 °C for 24 h to receive $FeCo_2S_4$ (Liao et al., 2022).

2.3.2 GO synthesis

Graphene oxide was prepared using Hummers' method. Firstly, a four-neck flask containing 3 g of graphite powder was put in an ice bath. Then, 75 mL H_2SO_4 (98%) was slowly added to the flask, stirring the suspension for 1 h. Next, 9 g of $KMnO_4$ was slowly added to the mixture under continuous stirring. After 3 h, 100 mL of deionized (DI) water was dropped slowly into the mixture, then an additional 150 mL of DI water was added. Finally, 20 mL of hydrogen peroxide (30%) was slowly poured into the mixture and stirred for 30 min on the ice bath. Subsequently, the mixture was washed with DI water and centrifuged until its pH was approximately neutral. GO was then freeze-dried and kept in cold conditions for further experiments (Le et al., 2022).

2.3.3 Synthesis of activated carbon from biowaste

Micronized BSG was mixed with distilled water in a 1:6 ratio to achieve a homogeneous solution. The resulting mixture was then transferred to a stainless-steel autoclave reactor with a total volume of 90 mL. The reaction underwent thermal treatment at 180 °C for 3 h and was cooled to room temperature. The solid material was then dried in an oven at 110 °C for 24 h, and the final product was designated as HT-180.

The activation and pyrolysis processes proceeded: HT-180 was combined with KOH in a 1:2.5 ratio using a magnetic stirrer to create a homogeneous solution. This mixture was poured into a petri dish and dried in an oven at 110 °C until completely dry. The dried material was weighed and transferred into a GSL-1600X tubular furnace (Carbolite Gero, Germany) set at 800 °C under argon flow, with a heating ramp of 5 °C/min, and maintained for 8–12 h. Once carbonization was complete, the furnace was cooled to below 100 °C at room temperature. The carbonized BSG material was then ball-milled to obtain micro-sized particles, followed by washing with 3% HCl and distilled water until a pH of approximately 7 was achieved. The sample was dried at 105 °C for 12 h, and the final product was labeled AC.

2.3.4 Synthesis of composites

A mixture of 0.02 g $FeCo_2S_4$ and 5.59 g GO suspension (17.89 mg/mL), with a mass ratio of the composite between rGO and $FeCo_2S_4$ of 1:0.2, was sonicated for 60 min. The content was then transferred to an autoclave, heated to 160 °C for 5 h, and cooled to room temperature. The hybrid hydrogel was collected, washed several times with DI water, and kept in 10 mL of DI water. The residue was then freeze-dried to receive rGO/$FeCo_2S_4$.

In the comparison with the AC effect on the working performance of the SC, the ratio of the mixture was changed so that 0.02 g $FeCo_2S_4$ and 0.04 g of AC were mixed into 3.354 g of GO suspension (mass ratio rGO/AC/$FeCo_2S_4$ is 0.6/0.4/0.2). The mixture followed the hydrothermal reaction procedure and was freeze-dried to acquire rGO/AC/$FeCo_2S_4$.

According to the literature, polyaniline (PANI) was incorporated into the composite structure via the *in situ* polymerization method. A synthesized piece of rGO/$FeCo_2S_4$ or rGO/AC/$FeCo_2S_4$ was immersed in 50 mL of DI water in a 100 mL beaker, and 1.5 mL of aniline was added to the mixture. The solution was left to stand at room temperature for 2 h before the hydrogel piece was removed. This process was repeated before immersing the hydrogel piece in 50 mL of 6.8% perchloric acid for 18 h. Subsequently, the sample was placed in 22 mL of 9.2% perchloric acid and maintained at 0 °C for 1 h. An ammonium persulfate solution (17.5 mM, 10 mL) was gradually added to the perchloric acid solution under continuous stirring, while the sample was protected with a shell to prevent destruction. The mixture was kept at 0 °C for 24 h to allow polymerization. The resulting samples were thoroughly rinsed with DI water and freeze-dried to produce rGO/$FeCo_2S_4$@PANI and rGO/AC/$FeCo_2S_4$@PANI composites (Le et al., 2022).

2.4 Fabrication of working electrodes and electrochemical testing

The electrochemical test was performed by making a slurry with the crushed composite with a solution of PTFE (10% of total mass) in 1 mL of ethanol. The slurry was coated as a circle of 0.25 cm radius on the titanium mesh and then compressed under the pressure of 8 MPa using the Redats compressor. The electrochemical performance of the as-prepared electrodes was characterized using cyclic voltammetry (CV), galvanostatic charge-discharge (GCD) tests, and electrochemical impedance spectroscopy (EIS) techniques on a potentiostat Autolab PGSTAT-128 N at room temperature. Electrochemical measurements were performed in a three-electrode cell using a working electrode, a platinum wire counter electrode, and an Ag/AgCl reference electrode. The measurements were carried out in an aqueous solution of electrolytes of 1 M H_2SO_4 at room temperature.

Electrochemical impedance spectroscopy (EIS) measurements were conducted on aerogel structure-coated electrodes in a constant voltage mode (0.02 V vs. Ag/AgCl) by sweeping frequencies from 100 kHz to 0.01 Hz at an amplitude of 0.01 V root mean square voltage.

In the two-electrode system, two identical electrodes were compressed and placed into a Swagelok cell and separated by a piece of polymeric separator (NKK-MPF30AC). The same electrolyte of 1 M H_2SO_4 was used. The cycling stability of the prepared materials was measured in a two-electrode system by a BioLogic battery testing unit (BCS-810) at a current density of 2 A/g for 5,000 cycles.

3 Results and discussion

rGO has been reported to exhibit excellent electrical conductivity, short diffusion distances, and robust thermal and chemical stability. However, the structure of rGO is composed of graphene sheets that tend to re-stack due to van der Waals interactions between adjacent layers. This re-stacking phenomenon

can lead to irreversible capacity loss and a reduction in surface area. To address this limitation, this study fabricated aerogels composed of rGO and $FeCoS_4$ nanoparticles. In addition to structural challenges, the high production cost of graphite poses a significant barrier. Despite their promise for electrochemical applications, materials like graphite, GO, and rGO are expensive and often require labor-intensive processes under hazardous conditions.

The synergistic integration of rGO with sulfide materials offers a potential solution. $FeCoS_4$, utilized as a spacer in the aerogel structure, prevents the agglomeration and re-stacking of rGO sheets while enhancing the surface area. Moreover, incorporating the AC from biowaste collected from local breweries into the aerogel structures for supercapacitor electrode decipher its effect on the working performance of SC. With its flexibility and high conductivity, AC has significantly improved the performance of various electrochemical devices. However, the utilization of biowaste could contribute to environmental matters. The AC was synthesized separately and combined with rGO to form composites. Polyaniline (PANI) was also synthesized *in situ* within the aerogel structure.

3.1 Structure study of composites

The X-ray diffraction (XRD) patterns of biomass after the hydrothermal reaction displayed prominent peaks at 20° and 47° (Supplementary Figure S1) corresponding to the C (002) and C (100) planes of amorphous carbon. These peaks are characteristic of condensed aromatic carbonized planes (Gopalakrishnan and Badhulika, 2020). During the subsequent KOH activation process, potassium compounds such as K_2CO_3, K_2O, and K intercalated into the carbon structure. These compounds were later removed by rinsing with HCl, resulting in highly porous activated carbon with a high surface area (Nandi et al., 2023). The sharper peaks indicate greater aromatic ring condensation within the activated carbon (Avramiotis et al., 2021). After activation, the XRD patterns exhibited a new peak at 34.42°, likely corresponding to the (311) plane (Rodrigues et al., 2020).

The $FeCo_2S_4$ material crystallizes in a typical spinel structure, which belongs to the face-centered cubic (FCC) system with the Fd-3m space group. In this structure, Fe^{2+} and Co^{3+} ions occupy the tetrahedral and octahedral sites within a close-packed sulfide lattice. It was confirmed to be face-centered cubic (FCC) based on the allowed reflections obtained via XRD analysis (Figure 1a). The Miller indices ($h^2 + k^2 + l^2$) were calculated to determine the possible crystal planes of $FeCo_2S_4$. Prominent diffraction peaks observed at 18.05°, 21.25°, 29.73°, 35.05°, 36.59°, 41.35°, 46.45°, 56.15°, 61.66°, and 74.02° were indexed to the (111), (200), (311), (222), (400), (331), (333), (440), and (622) planes, respectively.

The FT-IR spectra of composites comprising rGO, $FeCo_2S_4$, AC, and PANI are presented in Figure 1b. Due to the similarity in their structures, the FT-IR peaks appeared comparable across the samples. When graphene oxide (GO) is reduced to rGO, carbonyl groups (C=O) are reduced to methylene (-CH_2-), as evidenced by the symmetric and asymmetric stretching vibrations of -CH_2- at 2,992 cm^{-1} and 2,908 cm^{-1}, respectively (Du et al., 2018). The stretching vibration of the C=C plane is observed at 1,550 cm^{-1}, while the sp^2 carbon stretching vibration of C=O, attributed to carboxylic groups at the edge of GO, appears at 1731 cm^{-1} (Kim et al., 2021). Strong peaks at 1,500 cm^{-1} correspond to aromatic C=C in-plane vibrations in the rGO sheet. Additionally, the peak at 1,550 cm^{-1} indicates C=O stretching of carboxylic acids, and a broad peak at 2,837 cm^{-1} signifies the presence of CH_2 groups. The C-O-C bond appears at 1,064 cm^{-1}, with C=O stretching peaks at 700 cm^{-1} (Liu et al., 2017). For PANI, the FT-IR spectrum displays a characteristic peak at 3,400 cm^{-1}, corresponding to N-H stretching vibrations of its amino groups, and a peak at 2,465 cm^{-1} associated with N-H unsaturated amine groups. Peaks at 1,567 cm^{-1} and around 1,600 cm^{-1} represent the stretching vibrations of amine groups and the benzenoid ring C=C, respectively (Tabhane et al., 2021). The strong board peaks at 2,927 cm^{-1} are ascribed to Co-S of $FeCo_2O_4$ (Ma et al., 2019). The peak at 1,010 cm^{-1} is M-S stretching of $FeCo_2S_4$ (Zhao et al., 2020).

3.2 Morphology study of composites

The structure of $FeCo_2S_4$ within the integrated hybrid aerogel is depicted in Figure 2. In this composite, $FeCo_2S_4$ serves as a spacing agent, effectively preventing the aggregation of graphene sheets. The SEM image of $FeCo_2S_4$ (Figure 2a) reveals a multiple-sheet structure that is densely packed and interconnected. This morphology results from the evolution of a flower-like $FeCo_2O_4$ structure formed through a 12-h hydrothermal reaction (Saaid et al., 2022). Figure 2b presents SEM images of activated carbon (AC) derived from brewer's biowaste. The AC sample, prepared with a pre-carbonized carbon to KOH ratio of 1:2.5 and pyrolyzed at 800 °C for 2 h, exhibits a rough and highly porous surface. This porosity arises from gasification during activation, which produces K_2O, CO, CO_2, K_2CO_3, K, H_2, and H_2O (Mistar et al., 2020). At temperatures exceeding 700 °C, K_2O and K_2CO_3 are formed, etching the carbon skeleton via redox reactions. At 800 °C, metallic potassium (K) diffuses into the carbon matrix, further enhancing porosity. Subsequent rinsing with HCl dissolves potassium and its compounds, yielding a highly porous activated carbon structure. The mesoporous nature of the AC sample indicates a large specific surface area, making it an excellent candidate for applications requiring high-performance materials.

After the hydrothermal reaction, a composite of rGO/$FeCo_2S_4$ was successfully formed. The addition of activated carbon (AC) further modified the hybrid aerogel, incorporating polyaniline (PANI) through *in situ* polymerization. Freeze-drying was then performed to obtain the final materials, which were characterized using SEM to analyze their morphology. The rGO/$FeCo_2S_4$ composite exhibits a well-defined 3D microstructure consisting of interconnected rGO sheets (Figure 2c). With the addition of AC, due to their structural similarity, AC is well-dispersed within the composite, resulting in a uniform rGO/AC/$FeCo_2S_4$ structure (Figure 2d). Figures 2e,f show that PANI is observed coating the rGO sheets. The morphology of the composites conjugated with PANI changes due to the polymer being distributed across or intercalating between the surfaces of the rGO sheets and sulfide metal particles. The incorporation of PANI into the composites not only alters their morphology but also enhances the pseudocapacitance of the materials. This improvement contributes to the higher electrochemical performance of the composites, making them highly promising for energy storage applications (Kiefer et al., 2023).

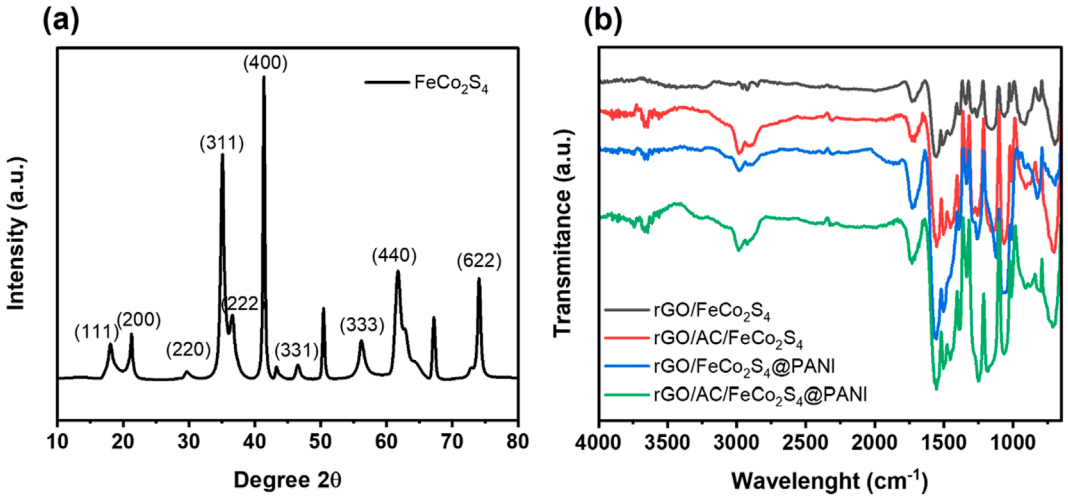

FIGURE 1
(a) XRD pattern of $FeCo_2S_4$ and **(b)** FT-IR spectrum of the composites.

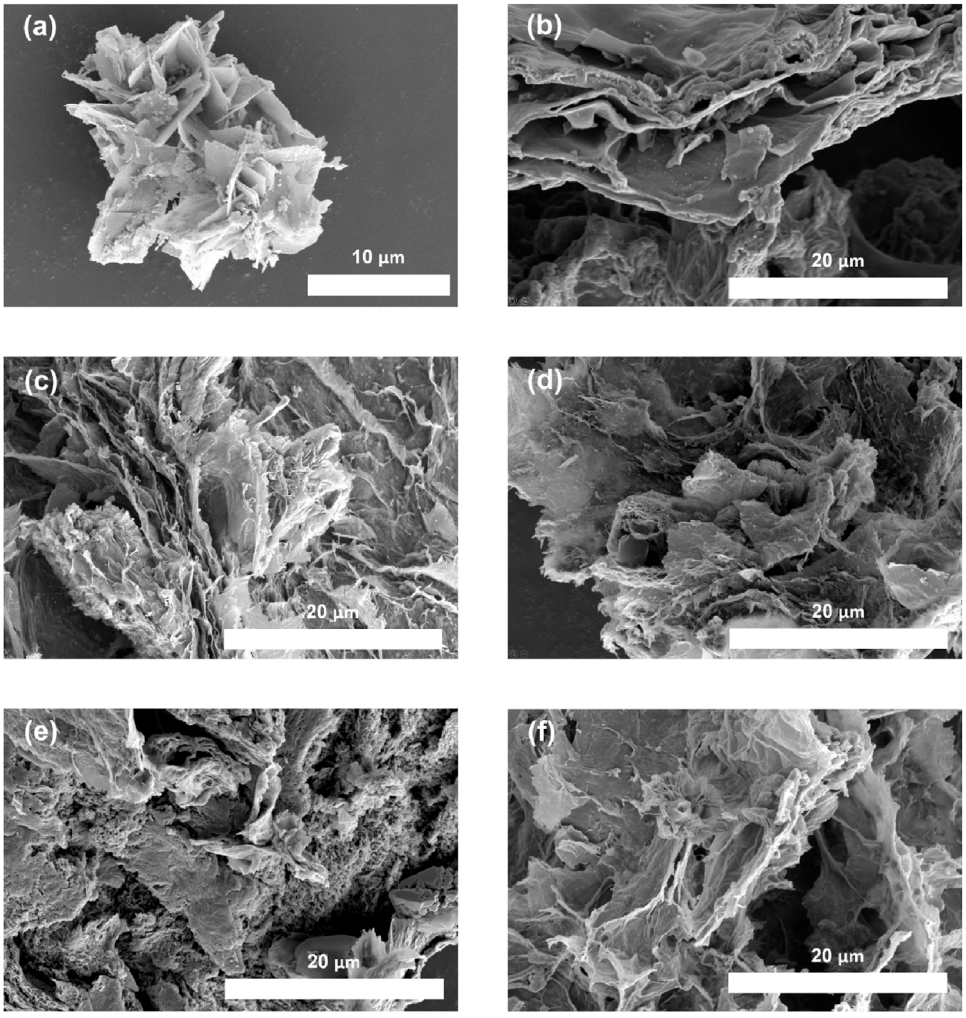

FIGURE 2
SEM images of **(a)** $FeCo_2S_4$, **(b)** AC, **(c)** $rGO/FeCo_2S_4$, **(d)** $rGO/AC/FeCo_2S_4$, **(e)** $rGO/FeCo_2S_4$@PANI, and **(f)** $rGO/AC/FeCo_2S_4$@PANI.

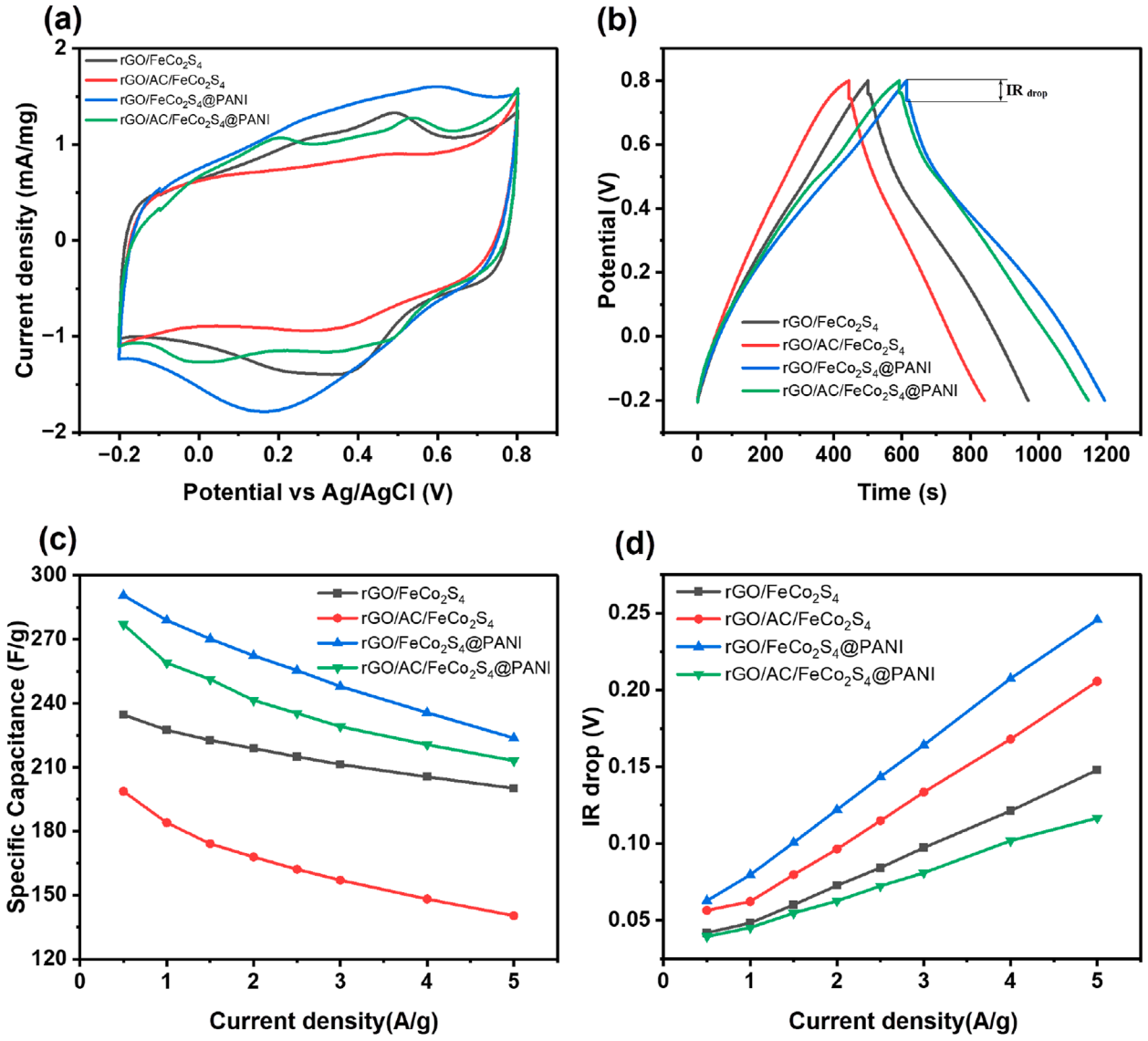

FIGURE 3
Electrochemical performance of **(a)** cyclic voltammetry at 5 mV/s, **(b)** GCD plots at 0.5 A/g, **(c)** specific capacitance calculated from GCD curves according to current densites, and **(d)** IR drop as a function of the current density of the electrodes made of composites.

3.3 Electrochemical performance of composites

The electrochemical properties of the composites were evaluated in a three-electrode system to analyze their performance as electrode materials, as shown in Figure 3. Supplementary Figure S2 further illustrates the cyclic-voltametry behavior of electrodes made from these composites. The experiments were conducted using a standard three-electrode setup, where cyclic voltammetry (CV) tests and galvanostatic charge-discharge (GCD) measurements were performed within a potential window of −0.2–0.8 V, using 1 M H_2SO_4 as the electrolyte.

At a scan rate of 5 mV/s, the CV spectra reveal that adding AC to the composites slightly reduces the CV curve area, leading to a decrease in the specific capacitance of the supercapacitor. This reduction can be attributed to the inherent characteristics of AC. While activated carbon is known for its large surface area, it typically exhibits lower capacitance compared to reduced graphene oxide (rGO), which possesses significantly better electrical conductivity and higher capacitance. This explains the observed decline in performance when AC is incorporated into the composites (Folaranmi et al., 2021).

The specific capacitance is directly proportional to the area under the CV curves, which decreases when AC is incorporated into the rGO/AC/$FeCo_2S_4$ composite. However, the CV area increases significantly when the composite is further modified with PANI, as shown in Figure 3a. This indicates a notable improvement in the specific capacitance of the rGO/AC/$FeCo_2S_4$@PANI composite. AC in the composite may hinder the electrolyte and electrode surface interaction, resulting in reduced charge transfer

efficiency. Figures 3b,d present the IR drop values at various current densities during the GCD tests. The IR drop represents the voltage loss due to internal resistance during current flow, causing energy dissipation as heat. A lower IR drop indicates higher efficiency and reduced thermal energy loss in the device. The GCD curves, measured within the potential range of −0.2–0.8 V, show that all samples exhibit nearly triangular shapes at a low current density of 0.5 A/g, indicating good capacitive behavior. However, as the current density increases, the IR drop in the GCD curves of all composites also increases. The rGO/AC/$FeCo_2S_4$ composite demonstrates a more pronounced IR drop, suggesting higher internal resistance compared to other samples. In contrast, conjugating PANI to the composite significantly reduces the resistance, resulting in a higher specific capacitance for rGO/AC/$FeCo_2S_4$@PANI. This highlights PANI's beneficial role in enhancing the composite's electrochemical performance.

The CV curves in Supplementary Figure S2 indicate that their shape changes progressively with increasing scan rates. This phenomenon occurs because, at higher scan rates, electrolyte ions lack sufficient time to diffuse into the inner active sites of the electrode (Le et al., 2021). We used a standard three-electrode system to perform CV tests within a fixed potential window of −0.2–0.8 V using 1 M H_2SO_4 as the electrolyte (Sekar et al., 2015). The response currents of all composite samples exhibit distinct redox peaks attributed to the faradic reactions of the electrode materials and carbon. The CV spectra of the samples at different scan rates, ranging from 5 to 100 mV/s, are presented in Supplementary Figure S2. Notably, electrodes fabricated from composites conjugated with PANI displayed higher current densities, indicating enhanced capacitance.

The CV curves for the rGO/$FeCo_2S_4$@PANI and rGO/AC/$FeCo_2S_4$@PANI composites revealed two pairs of redox peaks (Figure 3a), corresponding to surface reactions of PANI transitioning between its reduced state, partially oxidized state, and fully oxidized state (Wang et al., 2009). Doping in PANI involves the protonation of H^+ of the polymer backbone, which enhances its electrical conductivity. Counter ions, such as sulfate (SO_4^{2-}), balance the positive charges introduced during doping, maintaining electrical neutrality, as explained in the chemical (Equation 1).

$$(\mathrm{PANI})_n + ny\ \mathrm{SO_4^{2-}} \rightarrow \left[\mathrm{PANI^{y+}\,SO_4^{2-}}\right] + \mathrm{ny\ e^-} \quad (1)$$

Here, y represents the doping degree, defined as the ratio of charges in the polymer to the number of monomer units.

PANI exhibits excellent conductivity, enabling straightforward conversion between its oxidation states, emeraldine, leucoemeraldine, and pernigraniline, under current flow (Jugović et al., 2009). The CV spectra of conjugated composites highlight two redox peaks, indicating PANI's activity in acidic aqueous electrolytes. The first anodic peak is associated with doping H^+, representing the transition from PANI's leucoemeraldine form to emeraldine salt. The second peak corresponds to the transition of emeraldine to the fully oxidized pernigraniline state. This sequence underscores PANI's crucial role in enhancing the composites' electrochemical performance (Gospodinova and Terlemezyan, 1998).

GCD tests were conducted at different current densities from 0.5 A/g to 5 A/g (Figure 3b; Supplementary Figure S3) to further study the working performance of the composites enhanced with AC and PANI. The specific capacitance value was calculated, according to the Equation 2 as follows:

$$C_s = \frac{I.\Delta t}{m.\Delta V} \quad (2)$$

where I denotes the applied current (A), Δt is the time taken for the discharge, m is the mass of active electrode material, and ΔV is the discharge potential (Le et al., 2020).

The galvanostatic charge-discharge (GCD) curves of the composites revealed that at low current densities, the pseudocapacitive effect of polyaniline (PANI) integrated within the composites enabled rGO/$FeCo_2S_4$@PANI and rGO/AC/$FeCo_2S_4$@PANI to exhibit the best charge/discharge curves. This behavior indicates a higher specific capacitance compared to the other samples. However, with increasing current density, the accessibility of electrolyte ions to the electrode surface diminishes due to shortened interaction times (Brousse et al., 2006). The porous architecture of the composites plays a critical role in enhancing ionic conductivity, while the synergy among composite components facilitates efficient ion transport. This is corroborated by the SEM images (Figure 2), which display a highly porous surface morphology that promotes deep penetration of electrolyte ions into the internal structure of the composites. During charge/discharge cycles, these porous structures enable effective ion interaction with internal constituents such as rGO, PANI, and $FeCo_2S_4$. The combined effects of structural porosity and optimized material composition contribute significantly to the superior electrochemical performance observed in the composites.

Specific capacitance data for rGO/$FeCo_2S_4$@PANI, shown in Figure 3c, reveal notable variation with current density following the incorporation of PANI. At a current density of 0.5 A/g, rGO/$FeCo_2S_4$@PANI achieved the highest specific capacitance of 290.57 F/g, a considerable enhancement from the 234.62 F/g recorded for rGO/$FeCo_2S_4$ under the same conditions. The performance of composites containing AC is improved, where specific capacitance increased from 198.69 F/g to 277.03 F/g after PANI integration. This improvement suggests that the AC derived from biowaste interacts effectively with PANI and the electrolyte in supercapacitor applications.

Figure 3d presents the variation in IR drop at different current densities during GCD testing. The IR drop reflects the potential difference across a conducting phase during current flow, indicating resistive impedance (Mohamed et al., 2021). The GCD curves, recorded within a potential window of −0.2–0.8 V, exhibit nearly triangular shapes at low current density (0.5 A/g) across all samples. As the current density increases, the IR drop becomes more pronounced in all composites. Notably, rGO/$FeCo_2S_4$@PANI demonstrates the highest IR drop, indicating greater internal resistance than the other materials (Zhu et al., 2017). Nevertheless, the rGO/$FeCo_2S_4$@PANI electrode's strong electrochemical performance is attributed to PANI's high pseudocapacitance contribution.

3.4 Prototype SC application of composite

To further elucidate ion transport resistance, an equivalent circuit model was applied in Figure 4a. This model comprises Rs

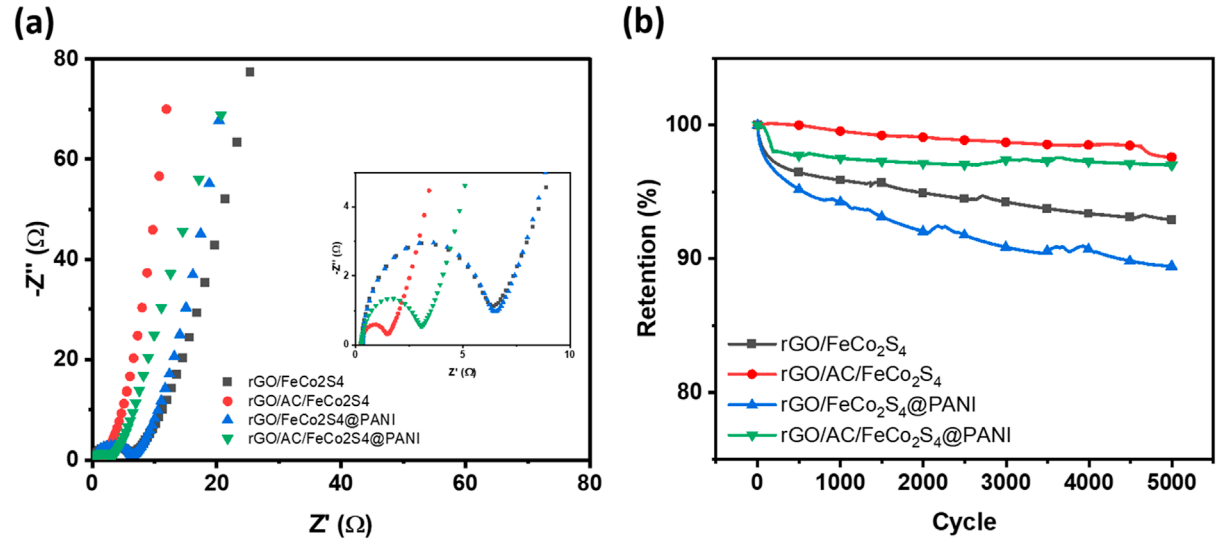

FIGURE 4
(a) Electrical impedance spectroscopy of the SCs made of composites, and **(b)** The cyclic capacity retention during 5,000 cycles at 2 A/g of symmetrical cell of composites.

(series resistance), Rct (charge transfer resistance), Cp (capacitance), and W (Warburg impedance), which characterizes ion diffusion behavior. The linear region observed in the low-frequency domain corresponds to Warburg impedance, where the slope of the oblique line reflects the efficiency of electrolyte ion diffusion. A steeper, more vertical trend implies lower diffusion resistance, indicating enhanced ion mobility within the composite electrodes. The near-linear behavior of composites in this region suggests reduced ion transport limitations, whereas the significant deviation seen in AC implies hindered ion diffusion (Ye et al., 2021).

A two-electrode symmetric supercapacitor setup was employed to investigate the ion transport mechanisms and retention within the composites. Figure 4a presents the Nyquist plots, with semicircles observed in the high and mid-frequency regions. Small Rct values indicate favorable capacitive behavior, with rGO/AC/$FeCo_2S_4$ exhibiting the lowest Rct (1.498 Ω), suggesting superior retention (Ye et al., 2021). In contrast, other composites show higher Rct values, which may signal reduced retention performance (Li et al., 2016). The slope of the oblique line in the low-frequency region represents the ion diffusion rate, where a long, straight imaginary axis indicates low diffusion resistance in the composite electrode material (Ye et al., 2021).

Figure 4b illustrates the cycling stability of the composites over 5,000 charge-discharge cycles at a current density of 2 A/g using a two-electrode symmetric supercapacitor configuration. Among the tested materials, rGO/$FeCo_2S_4$@PANI exhibits reduced cycling stability, primarily due to the mechanical degradation of PANI during repeated doping and dedoping processes. Continuous interaction between PANI and electrolyte ions throughout SC operation leads to molecular structural changes, resulting in the formation and subsequent release of H^+ and polymer complexes. These persistent redox reactions gradually degrade the polymer chains, compromising the composite's long-term structural and electrochemical stability (Rudolf et al., 2024).

In contrast, the improved capacitance retention observed in rGO/AC/$FeCo_2S_4$@PANI can be attributed to the stabilizing effect of AC. AC can form a more robust and stable matrix with PANI, mitigating the degradation typically seen in pure rGO/$FeCo_2S_4$@PANI composites (Le et al., 2022). The enhanced retention performance of AC-containing composites can also be linked to the mechanical stability provided by the AC's aerogel-like porous structure, which supports the active material during prolonged cycling (Li et al., 2016).

4 Conclusion

We successfully synthesized activated carbon (AC) from locally sourced brewery biowaste, demonstrating a sustainable and cost-effective approach to electrode material development. A composite comprising $FeCo_2S_4$, reduced graphene oxide (rGO), was fabricated via a one-step hydrothermal method. Conducting polymer of polyaniline (PANI) was conjugated within the structure via *in situ* polymerization. The composites were evaluated as electrode materials for supercapacitors using H_2SO_4 as the electrolyte. At low scan rates, the rGO/$FeCo_2S_4$@PANI composite exhibited the highest specific capacitance (290.57 F/g), attributed to the synergistic effect of EDLC and pseudocapacitance provided by rGO, PANI, and $FeCo_2S_4$. However, this composite suffered considerable capacitance loss after 5,000 cycles, primarily due to mechanical and structural degradation of PANI during repeated doping/dedoping. In contrast, the rGO/AC/$FeCo_2S_4$@PANI composite, despite having a slightly lower initial specific capacitance, demonstrated significantly improved cycling stability. The addition of biowaste-derived AC contributed to enhanced retention by providing a more stable structural framework and mitigating the degradation of PANI. Although AC did not markedly enhance the working performance in terms of capacitance, its role in improving long-term stability

underscores its importance in practical applications. These findings highlight the potential of incorporating sustainable materials like biowaste-derived AC into composite electrodes, offering a promising path toward durable, eco-friendly supercapacitors. Future research will focus on optimizing the composition and architecture of these hybrid materials to further enhance both performance and stability.

Data availability statement

The raw data supporting the conclusions of this article will be made available by the authors, without undue reservation.

Author contributions

AD: Conceptualization, Formal Analysis, Methodology, Writing – review and editing, Investigation. CB: Investigation, Resources, Writing – review and editing, Formal Analysis. VP: Data curation, Investigation, Validation, Visualization, Writing – review and editing. NK: Conceptualization, Methodology, Project administration, Resources, Writing – review and editing. PS: Conceptualization, Funding acquisition, Project administration, Resources, Supervision, Writing – review and editing. RK: Conceptualization, Formal Analysis, Visualization, Writing – review and editing, Investigation, Resources. QL: Funding acquisition, Investigation, Project administration, Resources, Supervision, Writing – original draft.

Funding

The author(s) declare that financial support was received for the research and/or publication of this article. The authors acknowledge the financial support provided by the Internal Grant Agency (IGA) projects IGA/CPS/2024/005 and IGA/CPS/2025/007 of the Center of Polymer Systems at the Tomas Bata University in Zlín. This work was supported by the Horizon Europe project TwinVECTOR of the European Union (Grant Agreement No. 101078935).

Conflict of interest

The authors declare that the research was conducted in the absence of any commercial or financial relationships that could be construed as a potential conflict of interest.

Generative AI statement

The author(s) declare that no Generative AI was used in the creation of this manuscript.

Any alternative text (alt text) provided alongside figures in this article has been generated by Frontiers with the support of artificial intelligence and reasonable efforts have been made to ensure accuracy, including review by the authors wherever possible. If you identify any issues, please contact us.

Publisher's note

Supplementary material

The Supplementary Material for this article can be found online at: https://www.frontiersin.org/articles/10.3389/fenrg.2025.1663842/full#supplementary-material

References

Abdullah, T., Shamsah, S. I., Shaaban, I. A., Akhtar, M., and Yousaf, S. (2023). Engineering energy storage properties of rGO based Fe2O3/CuO/PANI quaternary nanohybrid as an ideal electroactive material for hybrid supercapacitor application. *Synth. Met.* 299, 117472. doi:10.1016/J.SYNTHMET.2023.117472

Abioye, A. M., and Ani, F. N. (2015). Recent development in the production of activated carbon electrodes from agricultural waste biomass for supercapacitors: a review. *Renew. Sustain. Energy Rev.* 52, 1282–1293. doi:10.1016/J.RSER.2015.07.129

Avramiotis, E., Frontistis, Z., Manariotis, I. D., Vakros, J., and Mantzavinos, D. (2021). Oxidation of sulfamethoxazole by rice husk biochar-activated persulfate. *Catalysts* 11, 850. doi:10.3390/CATAL11070850

Bakhoum, D. T., Oyedotun, K. O., Sarr, S., Sylla, N. F., Maphiri, V. M., Ndiaye, N. M., et al. (2022). A study of porous carbon structures derived from composite of cross-linked polymers and reduced graphene oxide for supercapacitor applications. *J. Energy Storage* 51, 104476. doi:10.1016/J.EST.2022.104476

Basnayaka, P. A., Ram, M. K., Basnayaka, P. A., and Ram, M. K. (2017). A review of supercapacitor energy storage using nanohybrid conducting polymers and carbon electrode materials. In: *Conducting Polymer Hybrids*. Cham: Springer. p. 165–192. doi:10.1007/978-3-319-46458-9_6

Brousse, T., Toupin, M., Dugas, R., Athouël, L., Crosnier, O., and Bélanger, D. (2006). Crystalline MnO[sub 2] as possible alternatives to amorphous compounds in electrochemical supercapacitors. *J. Electrochem Soc.* 153, A2171. doi:10.1149/1.2352197

Chen, Z., Li, Z., Zhang, M., Wang, Y., Zhang, S., Cheng, Y., et al. (2024). Preparation of non-noble metal catalyst FeCo2O4/MoS2 for production of hydrogen and oxygen by electrochemical decomposition of water. *Inorganics* 12, 229. doi:10.3390/INORGANICS12080229

Delewary, A. R., Fei, H., Ngwabebhoh, F. A., Bubulinca, C., and Saha, P. (2025). Enhancing supercapacitor energy density via KMnO4-activated apple waste-derived carbon and aqueous trifluoroacetic acid electrolyte. *Biomass. Bioener* 201, 108142. doi:10.1016/J.BIOMBIOE.2025.108142

Du, F. P., Cao, N. N., Zhang, Y. F., Fu, P., Wu, Y. G., Lin, Z. D., et al. (2018). PEDOT:PSS/graphene quantum dots films with enhanced thermoelectric properties via strong interfacial interaction and phase separation. *Sci. Rep.* 8, 6441–12. doi:10.1038/s41598-018-24632-4

Fasakin, O., Dangbegnon, J. K., Momodu, D. Y., Madito, M. J., Oyedotun, K. O., Eleruja, M. A., et al. (2018). Synthesis and characterization of porous carbon derived from activated banana peels with hierarchical porosity for improved electrochemical performance. *Electrochim Acta* 262, 187–196. doi:10.1016/J.ELECTACTA.2018.01.028

Folaranmi, G., Bechelany, M., Sistat, P., Cretin, M., and Zaviska, F. (2021). Activated carbon blended with reduced graphene oxide nanoflakes for capacitive deionization. *Nanomaterials* 11, 1090. doi:10.3390/nano11051090

Fu, H., Chen, L., Gao, H., Yu, X., Hou, J., Wang, G., et al. (2020). Walnut shell-derived hierarchical porous carbon with high performances for electrocatalytic hydrogen evolution and symmetry supercapacitors. *Int. J. Hydrogen Energy* 45, 443–451. doi:10.1016/J.IJHYDENE.2019.10.159

Gao, Y. (2017). Graphene and polymer composites for supercapacitor applications: a review. *Nanoscale Res. Lett.* 12, 387–17. doi:10.1186/S11671-017-2150-5

Gong, Y., Li, J., Jiang, P. G., Li, Q. F., and Lin, J. H. (2013). Novel metal(II) coordination polymers based on N,N′-bis-(4-pyridyl)phthalamide as supercapacitor electrode materials in an aqueous electrolyte. *Dalton Trans.* 42, 1603–1611. doi:10.1039/C2DT31965A

Gopalakrishnan, A., and Badhulika, S. (2020). Effect of self-doped heteroatoms on the performance of biomass-derived carbon for supercapacitor applications. *J. Power Sources* 480, 228830. doi:10.1016/J.JPOWSOUR.2020.228830

Gospodinova, N., and Terlemezyan, L. (1998). Conducting polymers prepared by oxidative polymerization: polyaniline. *Prog. Polym. Sci.* 23, 1443–1484. doi:10.1016/S0079-6700(98)00008-2

Jugović, B., Gvozdenović, M., Stevanović, J., Trišović, T., and Grgur, B. (2009). Characterization of electrochemically synthesized PANI on graphite electrode for potential use in electrochemical power sources. *Mater Chem. Phys.* 114, 939–942. doi:10.1016/J.MATCHEMPHYS.2008.10.069

Kiefer, R., Vo, P. N. X., Kazantseva, N. E., Saha, P., and Le, Q. B. (2023). *Redox-active polymeric materials applied for supercapacitors*. Singapore: Springer. p. 229–243. doi:10.1007/978-981-99-4193-3_13

Kim, J. H., Shim, G. H., Vo, T. T. N., Kweon, B., Kim, K. M., and Ahn, H. S. (2021). Building with graphene oxide: effect of graphite nature and oxidation methods on the graphene assembly. *RSC Adv.* 11, 3645–3654. doi:10.1039/D0RA10207E

Le, Q. B., Vargun, E., Fei, H., Cheng, Q., Bubulinca, C., Moučka, R., et al. (2020). Effect of PANI and PPy on electrochemical performance of rGO/ZnMn2O4 aerogels as electrodes for supercapacitors. *J. Electron Mater* 49, 4697–4706. doi:10.1007/S11664-020-08198-4

Le, Q. B., Nguyen, T. H., Fei, H., Sapurina, I., Ngwabebhoh, F. A., Bubulinca, C., et al. (2021). Electrochemical performance of composites made of rGO with Zn-MOF and PANI as electrodes for supercapacitors. *Electrochim Acta* 367, 137563. doi:10.1016/J.ELECTACTA.2020.137563

Le, Q. B., Nguyen, T. H., Fei, H., Bubulinca, C., Munster, L., Bugarova, N., et al. (2022). Electrochemical performance of composite electrodes based on rGO, Mn/Cu metal–organic frameworks, and PANI. *Sci. Rep.* 12, 664–13. doi:10.1038/s41598-021-04409-y

Le, Q. B., Kiefer, R., Vo, P. N. X., Kazantseva, N. E., and Saha, P. (2024). Conducting polymers for pseudocapacitors. *Eng. Mater.* F1837, 157–175. doi:10.1007/978-3-031-45430-1_9

Li, M., Cheng, J. P., Wang, J., Liu, F., and Zhang, X. B. (2016). The growth of nickel-manganese and cobalt-manganese layered double hydroxides on reduced graphene oxide for supercapacitor. *Electrochim Acta* 206, 108–115. doi:10.1016/J.ELECTACTA.2016.04.084

Li, H., Chen, Q., Guo, H., Ji, D., Huang, Z., and Du, B. (2022). Synthesis of CoFe2O4/peanut shell powder composites and the associated magnetic solid phase extraction of phenoxy carboxylic acid herbicides in water. *Int. J. Environ. Res. Public Health* 19, 8450. doi:10.3390/IJERPH19148450

Liao, C. W., Chen, S. Y., Hsu, L. C., Lin, C. W., Chen, J. L., Kuo, C. H., et al. (2022). Insights into electrocatalytic oxygen evolution over hierarchical FeCo2S4 nanospheres. *ACS Sustain Chem. Eng.* 10, 431–440. doi:10.1021/ACSSUSCHEMENG.1C06658

Liu, Y., Liu, X., Dong, W., Zhang, L., Kong, Q., and Wang, W. (2017). Efficient adsorption of sulfamethazine onto modified activated carbon: a plausible adsorption mechanism. *Sci. Rep.* 7, 12437. doi:10.1038/S41598-017-12805-6

Ma, L., Abney, C. W., and Lin, W. (2009). Enantioselective catalysis with homochiral metal–organic frameworks. *Chem. Soc. Rev.* 38, 1248–1256. doi:10.1039/B807083K

Ma, D., Lv, M., Shen, Y., Zhu, Y., Wang, F., and Zhang, X. (2019). Fabrication of porous mesh-like FeCo2S4 nanosheet arrays on Ni foam for high performance all solid-state supercapacitors and water splitting. *ChemistrySelect* 4, 1879–1889. doi:10.1002/SLCT.201803107

Mistar, E. M., Alfatah, T., and Supardan, M. D. (2020). Synthesis and characterization of activated carbon from Bambusa vulgaris striata using two-step KOH activation. *J. Mater. Res. Technol.* 9, 6278–6286. doi:10.1016/J.JMRT.2020.03.041

Mohamed, S. G., Chen, C. J., Chen, C. K., Hu, S. F., and Liu, R. S. (2014). High-performance lithium-ion battery and symmetric supercapacitors based on FeCo2O4 nanoflakes electrodes. *ACS Appl. Mater Interfaces* 6, 22701–22708. doi:10.1021/am5068244

Mohamed, M. G., Ahmed, M. M. M., Du, W. T., and Kuo, S. W. (2021). Meso/microporous carbons from conjugated hyper-crosslinked polymers based on tetraphenylethene for high-performance CO2 capture and supercapacitor. *Molecules* 26, 738. doi:10.3390/MOLECULES26030738

Nandi, R., Jha, M. K., Guchhait, S. K., Sutradhar, D., and Yadav, S. (2023). Impact of KOH activation on rice husk derived porous activated carbon for carbon capture at flue gas alike temperatures with high CO2/N2 selectivity. *ACS Omega* 8, 4802–4812. doi:10.1021/ACSOMEGA.2C06955

Rodrigues, S. C., Silva, M. C., Torres, J. A., and Bianchi, M. L. (2020). Use of magnetic activated carbon in a solid phase extraction procedure for analysis of 2,4-dichlorophenol in water samples. *Water Air Soil Pollut.* 231, 294–13. doi:10.1007/S11270-020-04610-1

Rudolf, K., Sapurina, I., Bubulinca, C., Lukas, M., Delawary, A. R., Nikola, B., et al. (2024). Composite materials for supercapacitor electrodes utilizing polypyrrole nanotubes, reduced graphene oxides and metal–organic framework. *Curr. Sci.* 127, 537. doi:10.18520/cs/v127/i5/537-543

Saaid, F. I., Kasim, M. F., Yang, C. C., Kumar, A., Tseng, T. Y., and Winie, T. (2022). Flower-like nanosheets FeCo2O4 for application in supercapacitor and dye-sensitized solar cell. *J. Mater. Sci. Mater. Electron.* 33, 3648–3669. doi:10.1007/S10854-021-07557-Z

Sapurina, I., Bubulinca, C., Trchová, M., Prokeš, J., and Stejskal, J. (2021). Conducting polypyrrole and polypyrrole/manganese dioxide composites prepared with a solid sacrificial oxidant of pyrrole. *Synth. Met.* 278, 116807. doi:10.1016/J.SYNTHMET.2021.116807

Sekar, P., Anothumakkool, B., and Kurungot, S. (2015). 3D polyaniline porous layer anchored pillared graphene sheets: enhanced interface joined with high conductivity for better charge storage applications. *ACS Appl. Mater Interfaces* 7, 7661–7669. doi:10.1021/ACSAMI.5B00504

Tabhane, G. H., Giripunje, S. M., and Kondawar, S. B. (2021). Fabrication and dielectric performance of RGO-PANI reinforced PVDF/BaTiO3 composite for energy harvesting. *Synth. Met.* 279, 116845. doi:10.1016/J.SYNTHMET.2021.116845

Teo, E. Y. L., Muniandy, L., Ng, E. P., Adam, F., Mohamed, A. R., Jose, R., et al. (2016). High surface area activated carbon from rice husk as a high performance supercapacitor electrode. *Electrochim Acta* 192, 110–119. doi:10.1016/J.ELECTACTA.2016.01.140

Wang, D. W., Li, F., Zhao, J., Ren, W., Chen, Z. G., Tan, J., et al. (2009). Fabrication of graphene/polyaniline composite paper via *in situ* anodic electropolymerization for high-performance flexible electrode. *ACS Nano* 3, 1745–1752. doi:10.1021/NN900297M

Wang, Z., Huang, J., Guo, Z., Dong, X., Liu, Y., Wang, Y., et al. (2019). A metal-organic framework host for highly reversible dendrite-free zinc metal anodes. *Joule* 3, 1289–1300. doi:10.1016/J.JOULE.2019.02.012

Wang, J., Zhang, X., Li, Z., Ma, Y., and Ma, L. (2020). Recent progress of biomass-derived carbon materials for supercapacitors. *J. Power. Sour.* 451, 227794. doi:10.1016/J.JPOWSOUR.2020.227794

Wei, W., Cui, X., Chen, W., and Ivey, D. G. (2011). Manganese oxide-based materials as electrochemical supercapacitor electrodes. *Chem. Soc. Rev.* 40, 1697–1721. doi:10.1039/C0CS00127A

Xu, C., Xu, B., Gu, Y., Xiong, Z., Sun, J., and Zhao, X. S. (2013). Graphene-based electrodes for electrochemical energy storage. *Energy Environ. Sci.* 6, 1388–1414. doi:10.1039/C3EE23870A

Ye, Q., Luo, Y., Cen, Q., Dong, R., Luo, T., Xu, X., et al. (2021). *In situ* hybridization of polyaniline on Mn oxide for high-performance supercapacitor. *J. Energy Storage* 36, 102330. doi:10.1016/J.EST.2021.102330

Zhang, K., Zhang, L. L., Zhao, X. S., and Wu, J. (2010). Graphene/polyaniline nanofiber composites as supercapacitor electrodes. *Chem. Mater.* 22, 1392–1401. doi:10.1021/CM902876U

Zhao, C., and Zheng, W. (2015). A review for aqueous electrochemical supercapacitors. *Front. Energy Res.* 3, 128918. doi:10.3389/FENRG.2015.00023

Zhao, D., Dai, M., Zhao, Y., Liu, H., Liu, Y., and Wu, X. (2020). Improving electrocatalytic activities of FeCo2O4@FeCo2S4@PPy electrodes by surface/interface regulation. *Nano Energy* 72, 104715. doi:10.1016/j.nanoen.2020.104715

Zhu, H., Li, M., Wang, D., Zhou, S., and Peng, C. (2017). Interfacial synthesis of free-standing asymmetrical PPY-PEDOT copolymer film with 3D network structure for supercapacitors. *J. Electrochem Soc.* 164, A1820–A1825. doi:10.1149/2.1401707JES